

# Collision-induced radiative quenching and other disintegration modes of the $2s$ state of muonic hydrogen and deuterium atoms

V.P. Popov\* and V.N. Pomerantsev†

*Skobeltsyn Institute of Nuclear Physics, Lomonosov Moscow State University, 119991 Moscow, Russia*

(Dated: January 11, 2022)

The formation and various disintegration modes of  $2s$  states for muonic hydrogen and deuterium atoms at kinetic energies both above and below the  $2s - 2p$  threshold are studied. The cross sections of the collision-induced radiative quenching, elastic scattering, and Coulomb deexcitation of  $(\mu^- p)_{2s}$  and  $(\mu^- d)_{2s}$  atoms in collisions with ordinary hydrogen and deuterium atoms at collision energies below the  $2s - 2p$  threshold are calculated in the framework of the close-coupling approach. The basis set includes all open and closed channels corresponding to exotic-atom states with principal quantum number  $n$  from 1 up to 30. Results of these numerical quantum-mechanical calculations of cross sections are used as input data for detailed cascade calculations. The kinetics of atomic cascade for  $\mu^- p$  and  $\mu^- d$  atoms is studied in the wide range of the relative target densities,  $\varphi = 10^{-8} - 1$  applying the improved version of the cascade model. It is shown that the collision-induced radiative quenching gives a significant contribution to the total disintegration of the  $2s$  state of muonic atoms at energies below the  $2s - 2p$  threshold. The initial population of the  $2s$  state for both muonic hydrogen and deuterium atoms, absolute intensities and probabilities of the different disintegration modes as well as their lifetimes are calculated for the fractions with kinetic energies above and below the  $2s - 2p$  threshold. The obtained results are compared with the known experimental data.

PACS numbers:

## I. INTRODUCTION

The negatively charged muons stopped in  $H_2$  or  $D_2$  gaseous target form  $\mu^- p$  or  $\mu^- d$  atoms in highly excited states [1–3]. The formation of muonic atoms of hydrogen isotopes is followed by a number of the subsequent radiative and collisional processes. In the process of deexcitation, an  $\mu^- p$  or  $\mu^- d$  atom passes through many intermediate states until it reaches the ground state or weak decay of the meson occurs ( $\mu^- \rightarrow e^- + \bar{\nu}_e + \nu_{mu}$ ) in the excited state of the atom. During this deexcitation cascade, a fraction of  $\mu^- p$  or  $\mu^- d$  atoms reaches the  $2s$  state. The number of atoms reached  $2s$  state is determined by several factors: the initial  $(n, l, E)$ -distributions (e.g., see [4, 5]), the competition of collisional processes and radiative transitions during the deexcitation cascade, as well as the target temperature and density.

Muonic hydrogen and muonic deuterium atoms are of special interest among exotic atoms due to their simplest structure and possibility to investigate a number of problems both the exotic atom physics and the bound-state QED. The  $2s$  state plays a particular role in these atoms due to  $(2s - 2p)$  Lamb shift,  $E_L = 202.0$  meV, and has no analog in hadronic atoms. A high-energy component of  $(\mu p)_{1s}$  with kinetic energy  $\sim 0.9$  keV was discovered [6, 7] from the analysis of the time-of-flight spectra (at low gas pressures  $p_{H_2} = 16$  and  $64$  hPa) and attributed to non-radiative quenching of the  $2s$  state due to the formation of the muonic molecule in a resonant  $(\mu p)_{2s} + H_2$  collision and subsequent Coulomb deexcitation of the  $(pp\mu)^+$  complex (see [8] and references therein). Theoretical estimation of the quenching rate in the framework of this model gives  $\sim 5 \times 10^{10} s^{-1}$  at liquid-hydrogen density

(LHD =  $4.25 \times 10^{22}$  atoms/cm<sup>3</sup>) that is about an order of magnitude smaller than the value  $4.4_{-1.8}^{+2.1} \times 10^{11} s^{-1}$  extracted from experiments [7]. In our paper [4] the observed collisional quenching and high-energy  $(\mu p)_{1s}$  component was explained by the direct Coulomb deexcitation (CD) process,

$$(\mu^- p)_{2s} + H \rightarrow (\mu^- p)_{1s}(0.9\text{keV}) + H, \quad (1)$$

The problem of the  $(\mu^- p)_{2s}$  collisional quenching in the hydrogen target has been studied previously both experimentally [6, 9–13] and theoretically [4, 14–18]. Experimental investigations with muonic hydrogen and deuterium atoms at Paul Scherrer Institute [19–22] performed at a low gas pressure have revived interest in the subject of the formation and disintegration modes of  $(\mu^- p)_{2s}$  and  $(\mu^- d)_{2s}$  atoms at kinetic energies both above and below the  $2s - 2p$  threshold.

The theoretical description of the collisional processes and kinetics of the atomic cascade was improved significantly in our works (e.g., see [4, 5, 23–28] and refs. therein).

In the collision of muonic hydrogen or deuterium atoms in the  $2s$  state with the target atom or molecule, a strong coupling between this state and the unstable with respect to the radiative  $2p \rightarrow 1s$  transition  $2p$  state leads to the collision-induced radiative quenching of the  $2s$  state at kinetic energies below the  $2s - 2p$  threshold. The consequences of this mechanism can be observed in both the absolute x-ray yield of the  $K\alpha$  line and the lifetime of the muonic hydrogen and deuterium atoms in the  $2s$  state. According to our knowledge, the process of the collision-induced radiative quenching of the  $(\mu p)_{2s}$  state has been treated in the framework of the semiclassical approaches [15, 17] and was never taken into account in cascade calculations, since the delayed  $K_\alpha$  x-rays induced during the collisions have not been experimentally observed [11].

In this paper, we investigate the further history of  $(\mu^- p)$  and  $(\mu^- d)$  atoms formed in the  $2s$  state with ki-

\*Electronic address: vlad.popov1945@mail.ru

†Electronic address: pomeran@nucl-th.sinp.msu.ru

netic energies both above and below the  $2s-2p$  threshold. Their fate is determined by the interplay of a few processes: the elastic  $2s-2s$  scattering, the  $2s \rightarrow 2p$  Stark transition followed by the fast radiative  $2p \rightarrow 1s$  deexcitation, the collision-induced radiative quenching, the Coulomb deexcitation  $2s \rightarrow 1s$ , and  $\mu$ -decay.

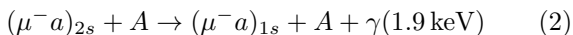
The paper is organized as follows. Section II presents the results of calculations of the cross sections for elastic  $2s-2s$  scattering,  $2s-2p$  Stark transitions, collision-induced radiation quenching, and  $2s-1s$  Coulomb deexcitation for muonic hydrogen and deuterium atoms performed in the framework of the close-coupling approach. Results of cascade calculations are presented in Sec. III. Initial populations and kinetic energy distributions of  $(\mu^-p)_{2s}$  and  $(\mu^-d)_{2s}$  atoms are presented in Sec. III A. Collisional rates for  $(\mu^-p)_{2s}$  and  $(\mu^-d)_{2s}$  atoms and intensities of the different modes of their disintegration are given in Secs. III B and III C, correspondingly. The contributions of different processes, forming the absolute x-ray yield of  $K\alpha$  line are discussed in Sec. III D. Calculated probabilities of different disintegration modes and a lifetime of  $(\mu^-p)_{2s}$  and  $(\mu^-d)_{2s}$  atoms with energies both above and below the  $2s-2p$  threshold are presented in Sec. III E. The results are summarized in Sec. IV.

Atomic units are used throughout unless otherwise stated.

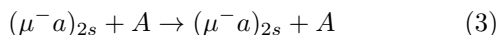
## II. CROSS SECTIONS OF COLLISIONAL PROCESSES FOR MUONIC HYDROGEN AND DEUTERIUM ATOMS

In our paper [5], the cross sections of all processes at collisions of the excited  $\mu^-p$  and  $\mu^-d$  atoms with hydrogen isotope atoms in the ground state have been presented. In these calculations, performed in the framework of the close-coupling approach, the radiative widths or instability of the excited states of muonic atoms and the possibility of the collision-induced radiative transitions were not taken into account. This approximation is completely justified for all excited  $nl$  states except the  $2p$  state. Indeed, the radiative widths of highly excited states are very small and the rates of the collision-induced radiative transitions are negligible compared to the rate of the direct radiative dipole transitions  $nl \rightarrow n'l \pm 1$ .

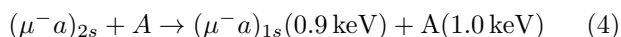
The situation is quite different in the case of the  $2s$  state. At collision energies below the  $2s-2p$  threshold, the Stark transition  $2s \rightarrow 2p$  is energetically forbidden and the collision-induced radiative quenching



( $a = p$  or  $a = d$ , and  $A = H, D$ ) may prove to be an important mechanism of the disintegration of the  $2s$  state. Therefore, in this paper devoted to the fate of the  $2s$  state in muonic hydrogen and deuterium atoms, the cross sections of the elastic scattering



and Coulomb deexcitation (CD)



in  $(\mu^-p)_{2s} + H$  and  $(\mu^-d)_{2s} + D$  collisions calculated earlier [4, 5] at energies below the  $2s-2p$  threshold were recalculated taking into account the radiation width or the instability of the  $2p$  state.

Calculations were performed in the framework of the closed coupling approach by using the propagation matrix method described in details in our paper [4]. The main advantage of this method is that it allows to describe both open and closed unstable-state channels as well as to avoid numerical errors caused by the exponentially increasing linearly-independent solutions of the system of the close-coupling equations. This method has been developed and applied earlier by the authors, in particular, for the description of the collision-induced absorption or annihilation in the case of hadronic atoms [27, 28].

The present calculations were performed with the extended basis set including all states of the muonic hydrogen (deuterium) atom with the principal quantum number values from  $n = 1$  up to  $n_{max} = 30$ . The value  $\Gamma_{2p} = 80 \mu\text{eV}$  of the radiative width of the  $2p$  state was used for both muonic hydrogen and muonic deuterium atoms. All other states were considered as stable ones. In the case of the  $2s$  state at kinetic energies below the  $2s-2p$  threshold, the  $S$  matrix in the subspace of the open channels is not unitary due to the instability of the  $2p$  state. The unitary defect allows to determine the cross section of the collision-induced radiative transition from the  $2s$  state as follows:

$$\sigma_{2s}^{\text{ind}} = \frac{\pi}{k^2} \sum_{J, n'=1,2} (2J+1) \left( \delta_{2sJ, n'sJ} - |S_{2s \rightarrow n's}^J|^2 \right). \quad (5)$$

Here,  $k^2 = 2M_r E_{\text{cm}}$ ,  $E_{\text{cm}}$  is the relative motion energy in the entrance channel, and  $M_r$  is the reduced mass of the scattering problem.

Cross sections for  $(\mu^-p)_{2s} + H$  collisions calculated with  $\Gamma_{2p} = 80 \mu\text{eV}$  and  $\Gamma_{2p} = 0$  are shown in Fig. 1. As can be seen from Fig.1, the cross sections of the elas-

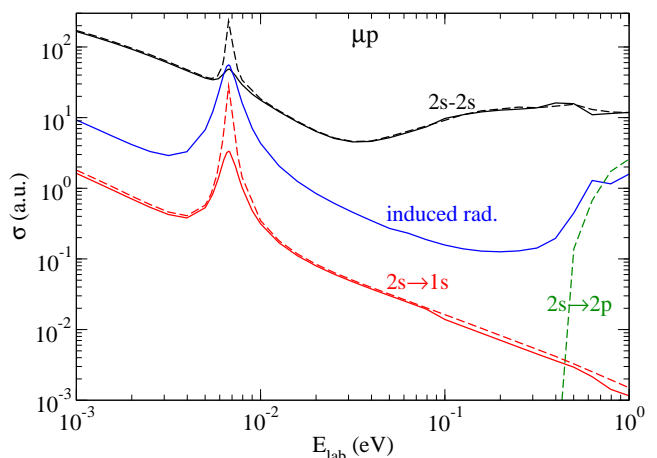


FIG. 1: The energy dependence of cross sections for  $(\mu^-p)_{2s} + H$  collisions: elastic scattering  $2s-2s$ , Coulomb deexcitation  $2s \rightarrow 1s$ , collision-induced radiative quenching, and Stark  $2s \rightarrow 2p$  transition. Cross sections of the elastic scattering and Coulomb deexcitation calculated with  $\Gamma_{2p} = 0$  [4] are shown by dashed lines for comparison.

tic scattering and CD practically do not change when the radiative width  $\Gamma_{2p}$  of the  $2p$  state is taken into account except for the resonance region. This means that the width can be considered as a small perturbation, and the cross section of the collision-induced process is proportional to the width. The dependence of the cross section of the collision-induced process on the value  $\Gamma$  has been studied in detail in our paper [28]. At the same time, in the resonance region, the cross sections of the elastic scattering and the CD are strongly suppressed (by several times in comparison with results presented in [4]) due to the process (2) of the collision-induced radiative quenching. In the resonance region, the cross section of the process (2) even exceeds the cross section of the elastic scattering.

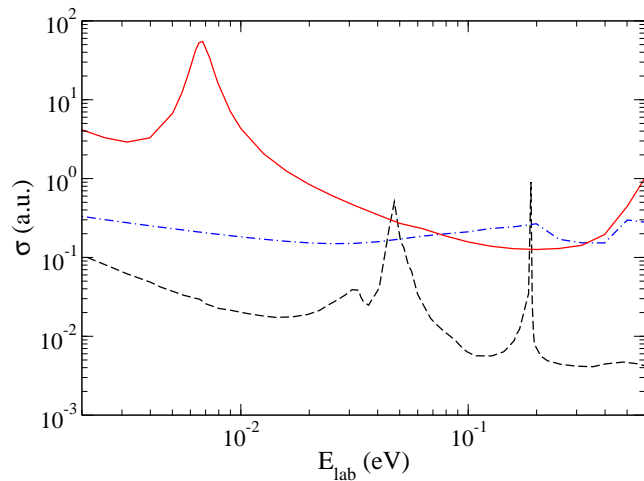


FIG. 2: Cross sections of the collision-induced radiative quenching for  $(\mu^-p)_{2s} + H$  collisions vs the laboratory kinetic energy below the  $2s - 2p$  threshold: the solid line and dashed-dotted line are the results of the present calculations with the basis sets  $n_{max} = 30$  and  $n_{max} = 2$ , respectively, and the dashed line is obtained from Fig. 4 of [17].

The comparison of the collision-induced radiative cross sections calculated in the present fully quantum-mechanical approach with the cross sections calculated in [17] within a simple model of the potential scattering with the complex potential is shown in Fig.2. Here the cross section of the collision-induced radiative quenching calculated with the simplest basis set in which only wave functions of the  $1s$ ,  $2s$ , and  $2p$  states of the muonic atom were included is also presented. In the paper [17], the Born-Oppenheimer approximation was applied using the four-term basis set with the lowest  $1s$  and  $2s$  orbitals in variational calculations. In such approximation, the scattering problem is reduced to a simple model of the potential scattering with the complex potential.

Figure 2 shows that the cross section of the collision-induced radiative quenching calculated in [17] is too small even in comparison with our close-coupling result obtained with the minimal basis set in which only the  $1s$ ,  $2s$ , and  $2p$  muonic-atom wave functions were taken into account. Besides, the cross section of collision quenching calculated in [15] is somewhat less in comparison with the result of [17]. Therefore, the adiabatic description and correspondingly the Born-Oppenheimer approximation is

not justified for the realistic treatment of the collision-induced radiative quenching of the  $2s$  state in  $(\mu^-p)_{2s} + H$  collisions at kinetic energies below the  $2s - 2p$  threshold.

Figure 3 shows the energy dependence of the cross sections for  $(\mu^-d)_{2s} + D$  collisions. In contrast to the case of the  $(\mu^-p)_{2s}$ , there are no pronounced sub-threshold resonances, and, therefore, taking into account the  $2p$ -state width does not at all affect the elastic scattering and CD cross sections.

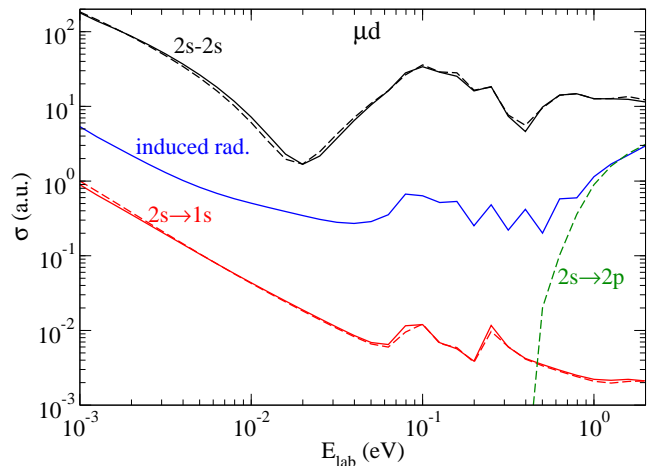


FIG. 3: The same as in Fig. 1 for  $(\mu^-d)_{2s} + D$  collisions. Cross sections of the elastic scattering and Coulomb deexcitation calculated with  $\Gamma_{2p} = 0$  from [5] are shown by dashed lines.

### III. RESULTS OF CASCADE CALCULATIONS

The cascade calculations for muonic hydrogen and muonic deuterium atoms were performed in the framework of the improved version of the cascade model developed in our recent papers [4, 5]. In particular, the probability densities of  $n$  and  $l$  initial (at the instant of the exotic atom formation) distributions as well as of the initial kinetic energy distribution (see Eqs. 22-24 in [5]) were used in the present cascade calculations. Besides, the exact kinematic of the binary collision taking into account the target motion was applied in the present cascade calculations (for detail see [5]). Finally, the present cascade model includes new results given in Sec. II for cross sections of the elastic scattering, collision-induced radiative quenching, and the CD for  $(\mu^-p)_{2s}$  and  $(\mu^-d)_{2s}$  at kinetic energies below the  $2s - 2p$  threshold.

To obtain good statistics, the fate of the  $10^8$  muonic atoms has been analyzed in the present cascade calculations for each value of the target density in the relative density range, covering nine orders of magnitude  $\varphi = 10^{-9} - 1$ , where  $\varphi$  is the target density in units of the liquid hydrogen density,  $N_{lhd} = 4.25 \cdot 10^{22}$  atoms/cm<sup>3</sup>.

The various characteristics of muonic hydrogen and deuterium atoms in the  $2s$  state were calculated: the arrival population and kinetic energy distribution, the intensities and probabilities of the different disintegration modes, and lifetimes. Some of present results are compared with the available experimental data [6, 11, 19, 22].

### A. Initial population and kinetic energy distribution of $(\mu^-p)_{2s}$ and $(\mu^-d)_{2s}$

We define the total initial or arrival population of the  $2s$  state,  $\varepsilon_{2s}^{\text{tot}}$ , as the probability that the formed muonic hydrogen or deuterium atom will reach this state during the deexcitation cascade regardless of whether its kinetic energy is above or below of the  $2s - 2p$  threshold.

The density dependence of the total arrival population for  $(\mu^-p)_{2s}$  and  $(\mu^-d)_{2s}$  atoms calculated using the present version of the atomic cascade is shown in Fig. 4. Calculations were performed at relative hydrogen density  $\varphi = (10^{-9} - 1)$  and at target temperature  $T = 300$  K.

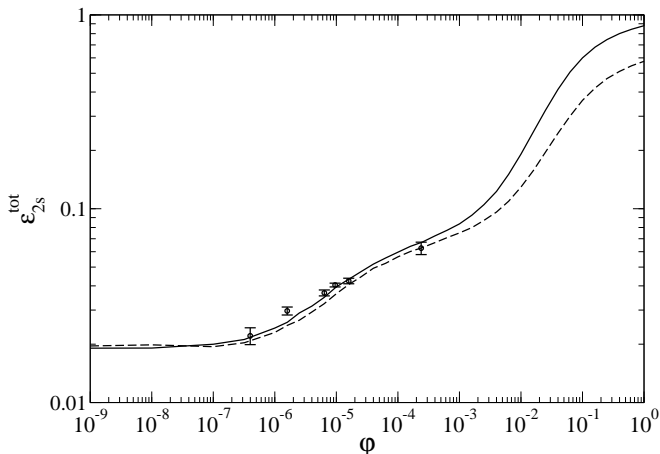


FIG. 4: The total arrival population  $\varepsilon_{2s}^{\text{tot}}$  of  $\mu^-p$  (solid line) and  $\mu^-d$  (dashed line) atoms vs the density of the target calculated at a target temperature  $T = 300$  K. The experimental data for are from [11].

The total arrival populations for the  $(\mu^-p)_{2s}$  and  $(\mu^-d)_{2s}$  have similar dependences on the target density. They are about 2% in the density range  $\varphi = (10^{-9} - 10^{-7})$  and grow up to 88% and 57% at a liquid hydrogen density for  $\mu^-p$  and  $\mu^-d$  atoms, respectively. In the case of muonic hydrogen the density dependence of the  $\varepsilon_{2s}^{\text{tot}}$  has been explained in detail in the paper [4]. The same explanation is also valid for the muonic deuterium.

At densities below  $10^{-7}$ , the role of collisional processes in the deexcitation cascade is extremely weak and the arrival population of the  $2s$  state is mainly determined by  $(n, l)$  distributions at the instant of the exotic atom formation and the rates of radiative transitions from the higher  $np$  states ( $n \geq 3$ ). So, in this density range, the arrival population  $\varepsilon_{2s}^{\text{tot}}$  is equal to about 2% and is very weakly dependent on the density for both muonic hydrogen and muonic deuterium atoms.

In the density range  $\varphi = 10^{-7} - 2.5 \cdot 10^{-4}$ , the arrival population  $\varepsilon_{2s}^{\text{tot}}$  increases from about 2% up to 6.77% and 6.34% for  $\mu^-p$  and  $\mu^-d$  atoms, respectively. In this density range, the total population of the  $2s$  state grows due to an increase of the intensity of all collisional processes, which in turn lead to a larger population of  $np$  states ( $n \geq 5$ ) and accordingly to an increase of the intensity of the radiative  $np \rightarrow 2s$  transitions.

This explanation is in accordance with the density dependence of the relative x-ray yields,  $Y_i = I(K_i)/I(K_{\text{tot}})$ ,

for  $K_i$  lines ( $i = \alpha, \beta, \gamma$ , etc) (see also Figs. 17 and 18 in [5]) and a strong correlation between the relative yields of  $K_i$  lines and the total population  $\varepsilon_{2s}^{\text{tot}}$ . At densities below  $2.5 \cdot 10^{-4}$ , the calculated arrival population  $\varepsilon_{2s}^{\text{tot}}$  is in perfect agreement with the estimation based on formula (see Eq. (21) in [4])

$$\varepsilon_{2s}^{\text{rad}} = 0.134(1 - Y_\alpha) + 0.01Y_{>\beta}. \quad (6)$$

At these densities, the calculated values of  $\varepsilon_{2s}^{\text{tot}}$  are in very good agreement with the experimental data obtained from the measured relative X-ray yields [11] at  $H_2$  gas pressures between 0.25 and 150 Torr ( $T = 300$  K) that corresponds to the range of the relative densities from  $3.8 \cdot 10^{-7}$  up to  $2.3 \cdot 10^{-4}$ .

At densities above  $2.5 \cdot 10^{-4}$ , the populations  $\varepsilon_{2s}^{\text{tot}}$  and  $\varepsilon_{2s}^{\text{rad}}$  have quite different dependencies on the density. The population  $\varepsilon_{2s}^{\text{rad}}$  reaches its maximum value 7.7% and 7.5% at  $\varphi = 2 \cdot 10^{-3}$  and then rapidly decreases to about 2.4% and 1.2% at  $\varphi = 1$ , respectively for  $\mu^-p$  and  $\mu^-d$  atoms. Contrary to this, the arrival population  $\varepsilon_{2s}^{\text{tot}}$  in the density range  $\varphi = 2 \cdot 10^{-3} - 1$  rapidly grows from 10.4% (for  $\mu^-p$ ) and 8.6% (for  $\mu^-d$ ) up to 88% and 57% at a liquid hydrogen density for  $\mu^-p$  and  $\mu^-d$  atoms, respectively. It is important to note, that these values of the total arrival population significantly exceed the statistical weight of the  $2s$  state (25%) especially in the case of the muonic hydrogen.

In the density range  $10^{-4} \lesssim \varphi \lesssim 3 \cdot 10^{-3}$ , Stark transitions increase the population of  $np$  states ( $3 \leq n \leq 5$ ) from which the radiative  $np \rightarrow 2s$  transitions populate the  $2s$  state. This explanation is supported by the density dependence of the absolute x-ray yields of the  $K\beta$ ,  $K\gamma$  and  $K\delta$  lines (see Fig. 15 in [5]).

At a density above  $\approx 3 \cdot 10^{-3}$ , the CD  $5 \rightarrow 4$ ,  $4 \rightarrow 3$ , and  $3 \rightarrow 2$  together with Auger and radiative transitions result in very fast increasing of the population  $\varepsilon_{2s}^{\text{tot}}$ . Besides, at the density  $\varphi \gtrsim 10^{-2}$  the rate of the Stark  $2p \rightarrow 2s$  transition is comparable with the rate of the radiative transition  $2p \rightarrow 1s$  and becomes even about two orders of the magnitude more at a liquid hydrogen density ( $\varphi = 1$ ). Therefore, at the density above  $10^{-2}$  the initial population of the  $2s$  state is mainly formed by the Auger transition  $3p \rightarrow 2s$ , the CD  $3l \rightarrow 2s$  ( $l = 0, 1, 2$ ), and the always open Stark  $2p \rightarrow 2s$  transition.

The kinetic energy of the muonic atom changes during the atomic cascade as a result of the complex interplay of various cascade processes preceding its arrival in the  $2s$  state. In cascade calculations, the kinetic energy distribution of exotic atoms at the time of their transition to the  $2s$  state is described by the probability density,  $\omega_{2s}(E; \varphi, T)$ , which is determined by the preceding cascade processes as well as by the target density and temperature.

In Fig. 5 we present the distribution function of the probability,

$$W_{2s}(E; \varphi, T) = \int_0^E \omega_{2s}(E'; \varphi, T) dE', \quad (7)$$

which determines the probability that the muonic atom has kinetic energy in the laboratory frame less than  $E$  at the instant of the  $2s$  state formation. Further, this

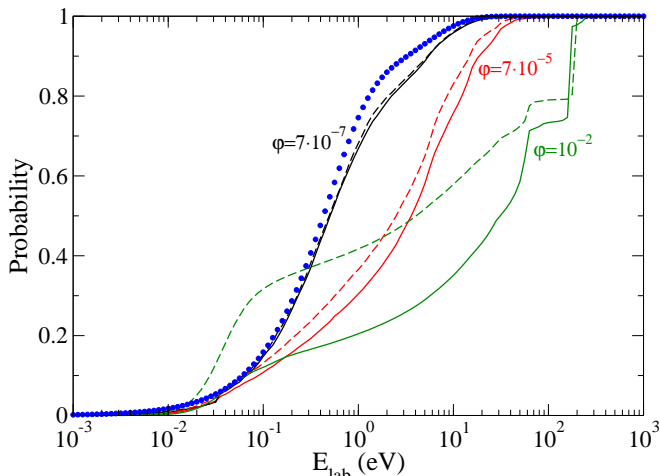


FIG. 5: Kinetic energy distributions of muonic hydrogen (solid lines) and deuterium (dashed lines) atoms on arrival in the  $2s$  state vs. the laboratory kinetic energy calculated at a target temperature  $T = 300$  K for three values of the relative target density:  $7 \cdot 10^{-7}$ ,  $7 \cdot 10^{-5}$  and  $10^{-2}$ . The dotted line corresponds to the initial energy distribution of muonic atoms at the instant of their formation (see Eq. (8)).

probability will be called the kinetic energy distribution of muonic hydrogen or muonic deuterium atoms on arrival in the  $2s$  state. Calculations were performed at a room target temperature  $T = 300$  K for three values of the relative target density:  $\varphi = 7 \cdot 10^{-7}$ ,  $7 \cdot 10^{-5}$ , and  $10^{-2}$ . The dotted line in the figure shows the kinetic energy distribution of muonic atoms at the instant of their formation, given by the formula

$$W_{\text{in}}(E) = 1 - \varkappa \exp(-E/E_1) - (1 - \varkappa) \exp(-E/E_2), \quad (8)$$

where parameters  $\varkappa = 0.805$ ,  $E_1 = 0.469$  eV, and  $E_2 = 4.822$  eV were determined in [4] from the fit of experimental data [6] at the density corresponding to the target pressure  $p_{\text{H}_2} = 0.0625$  hPa and temperature  $T = 300$  K.

As it is seen from Fig. 5, the kinetic energy distributions of the  $2s$  state for both muonic hydrogen and deuterium atoms are practically indistinguishable at the density  $\varphi = 7 \cdot 10^{-7}$  and have a small differences from the initial energy distribution given by Eq. (8). At very low target densities  $\varphi \lesssim 10^{-6}$  the deexcitation cascade is practically purely radiative and the initial kinetic energy distributions of muonic atoms at the instant of their formation are conserved up to the end of the cascade. In this density range the kinetic energy distributions of both muonic hydrogen and deuterium atoms in the  $2s$  state show a very small acceleration due to the Coulomb deexcitation of highly-excited states.

At densities  $\varphi \gtrsim 10^{-6}$ , the effect of the CD in the highly-excited states (preceding the population of the  $2s$  state) becomes more pronounced providing a high-energy component in the kinetic energy distribution of the  $2s$  state. In particular, at a density  $\varphi = 7 \cdot 10^{-5}$  (see Fig. 5), the contributions of the CD  $8 \rightarrow 7$ ,  $7 \rightarrow 6$ ,  $6 \rightarrow 5$ , and  $5 \rightarrow 4$  are explicitly seen in kinetic energy distributions of both  $(\mu^-p)_{2s}$  and  $(\mu^-d)_{2s}$  atoms. The

TABLE I: The density dependence of arrival populations  $\varepsilon_{2s}^a$  and  $\varepsilon_{2s}^b$  (per formed muonic atom) of  $(\mu^-p)_{2s}$  and  $(\mu^-d)_{2s}$  fractions above and below of the  $2s - 2p$  threshold, respectively.

$\varphi$ (lhd)	$(\mu^-p)_{2s}$		$(\mu^-d)_{2s}$	
	$\varepsilon_{2s}^a$ (%)	$\varepsilon_{2s}^b$ (%)	$\varepsilon_{2s}^a$ (%)	$\varepsilon_{2s}^b$ (%)
$10^{-8}$	1.06	0.87	1.05	0.88
$10^{-7}$	1.11	0.90	1.12	1.02
$10^{-6}$	1.48	0.98	1.48	1.03
$10^{-5}$	2.82	1.10	2.57	1.14
$10^{-4}$	4.64	1.28	4.10	1.41
$10^{-3}$	6.13	2.21	4.76	2.69
$10^{-2}$	15.74	3.35	7.89	4.95
$10^{-1}$	54.67	5.37	29.05	7.07
$10^0$	76.02	11.93	46.55	11.04

observed here small differences between kinetic energy distributions of  $(\mu^-p)_{2s}$  and  $(\mu^-d)_{2s}$  atoms are explained by the weak isotopic effect in cross sections of the CD for highly-excited states (for details see [5]). With the further density increasing the role of the CD becomes much more prominent. In particular, Figure 5 illustrates the significant isotopic effect of the CD in the kinetic energy distributions of the  $2s$ -state of muonic hydrogen and deuterium atoms at a density  $\varphi = 10^{-2}$ . Here the strong isotopic effect in the cross sections and accordingly in rates of the CD  $5 \rightarrow 4$ ,  $4 \rightarrow 3$ , and especially  $3 \rightarrow 2$  (e.g., see Figs. 8, 9, 11, and 12 in [5]) leads to significant differences in the kinetic energy distributions of atoms  $(\mu^-p)_{2s}$  and  $(\mu^-d)_{2s}$  at the instant of their formation.

In accordance with the kinetic energy distribution of the  $2s$  state (see Fig. 5) the total arrival population  $\varepsilon_{2s}^{\text{tot}}$  can be divided into two fractions

$$\varepsilon_{2s}^{\text{tot}}(\varphi) = \varepsilon_{2s}^a(\varphi) + \varepsilon_{2s}^b(\varphi), \quad (9)$$

where  $\varepsilon_{2s}^a(\varphi)$  and  $\varepsilon_{2s}^b(\varphi)$  denote arrival populations of fractions with the kinetic energy above and below the  $2s - 2p$  threshold, respectively. Absolute values of  $\varepsilon_{2s}^a(\varphi)$  and  $\varepsilon_{2s}^b(\varphi)$  calculated for  $(\mu^-p)_{2s}$  and  $(\mu^-d)_{2s}$  atoms at target densities from  $\varphi = 10^{-8}$  up to 1 and a target temperature  $T = 300$  K are shown in Table I.

It is important to notice some peculiarities in the formation of these fractions in muonic hydrogen and muonic deuterium atoms. First, the arrival population  $\varepsilon_{2s}^a$  for the muonic hydrogen and deuterium atoms with kinetic energies above the  $2s - 2p$  threshold is larger than the arrival population  $\varepsilon_{2s}^b$  with kinetic energies below the  $2s - 2p$  threshold at all values of the target density. Second, the arrival population  $\varepsilon_{2s}^a$  grows with the density much faster than the arrival population  $\varepsilon_{2s}^b$  for both  $(\mu^-p)_{2s}$  and  $(\mu^-d)_{2s}$  atoms. Finally, the arrival population  $\varepsilon_{2s}^b$  of the muonic deuterium is greater than the arrival population of the same fraction of the muonic hydrogen at all densities of the target except for the region very close to the liquid hydrogen density. On the contrary, at  $\varphi > 10^{-6}$ , the arrival population  $\varepsilon_{2s}^a$  for the muonic hydrogen is more (and even significantly more at  $\varphi \gtrsim 10^{-3}$ ) than the arrival population of the same fraction in the case of the muonic deuterium.

## B. Collisional rates of $(\mu^-p)_{2s}$ and $(\mu^-d)_{2s}$ atoms

After the formation of the hydrogen exotic atoms in the  $2s$  state, their further fate is determined by the rate of the muon decay ( $\lambda_\mu = 4.54 \cdot 10^5 \text{ ps}^{-1}$ ) and by the rates of the collisional processes: the elastic scattering  $2s - 2s$ , the collision-induced radiative quenching, the Stark transition  $2s \rightarrow 2p$  followed by the fast radiative transition  $2p \rightarrow 1s$ , and the CD  $2s \rightarrow 1s$ . The rate of the collisional process in the laboratory frame is defined as follows

$$\lambda_{nl \rightarrow n'l'}(E_{\text{lab}}) = \varphi N_{\text{LHD}} \sigma_{nl \rightarrow n'l'}(E_{\text{lab}}) \sqrt{\frac{2E_{\text{lab}}}{M}}, \quad (10)$$

where  $E_{\text{lab}}$  and  $M$  are the kinetic energy in the laboratory frame and the mass of the muonic atom, respectively.

Figure 6 shows the energy dependence of collisional rates for the elastic scattering  $2s - 2s$ , CD  $2s \rightarrow 1s$ , and collision-induced radiative quenching of the  $2s$  state for muonic hydrogen and deuterium atoms at the liquid hydrogen density ( $\varphi = 1$ ). The rate of the radiative transition  $\lambda^{\text{rad}}(2p \rightarrow 1s) = 0.12 \text{ ps}^{-1}$  is shown for comparison. A small difference of about 5% between radiative rates of the  $2p \rightarrow 1s$  transition in muonic hydrogen and deuterium due to the difference of their reduced masses is not visible at the scale of the figure.

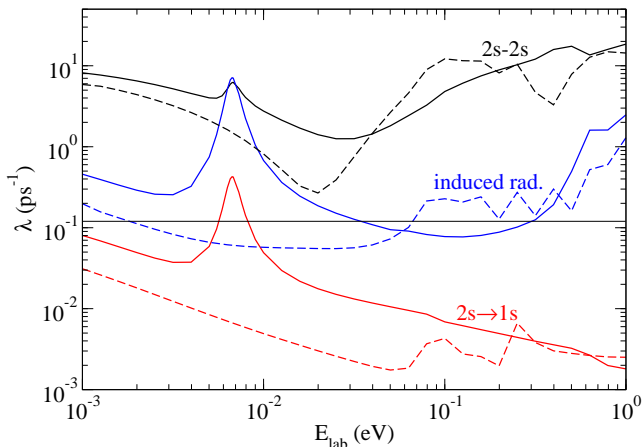


FIG. 6: Collisional rates of the elastic  $2s - 2s$  scattering, CD  $2s \rightarrow 1s$ , and collision-induced radiative quenching of the  $2s$  state as a function of the laboratory kinetic energy for  $(\mu^-p)$  (solid lines) and  $(\mu^-d)$  (dashed lines) atoms calculated at the liquid hydrogen density.

The isotope effect observed in cross sections for scattering of muonic atoms in states with values of the principal quantum number  $n < 8$  (see [5]) is practically absent for highly excited states with  $n > 8$ . The only source of the isotopic effect in the kinetics of the atomic cascade for states with  $n > 8$  is the trivial kinematic factor  $\sqrt{2E_{\text{lab}}/M}$  in Eq. (10). In the case of the  $2s$  state, the isotopic effect revealed in cross sections (see Figs. 1 and 3) is additionally enhanced by this factor associated with the difference of the exotic atom velocities at the same energy in the laboratory system. It is seen in Fig. 6, that the isotopic effect in rates of all collisional processes is very strong.

## C. Intensities of the different disintegration modes of $(\mu^-p)_{2s}$ and $(\mu^-d)_{2s}$

The intensities of the decay modes, i.e. the number of atoms (per one formed muonic atom) disintegrated through a given mode were calculated within the present cascade model for muonic hydrogen and deuterium atoms in  $2s$  state. The intensities of the destruction of the  $2s$  state for  $(\mu^-p)$  and  $(\mu^-d)$  atoms are shown as functions of the target density in Figs. 7 and 8, respectively, and are also presented in Tables II and III for several density values.

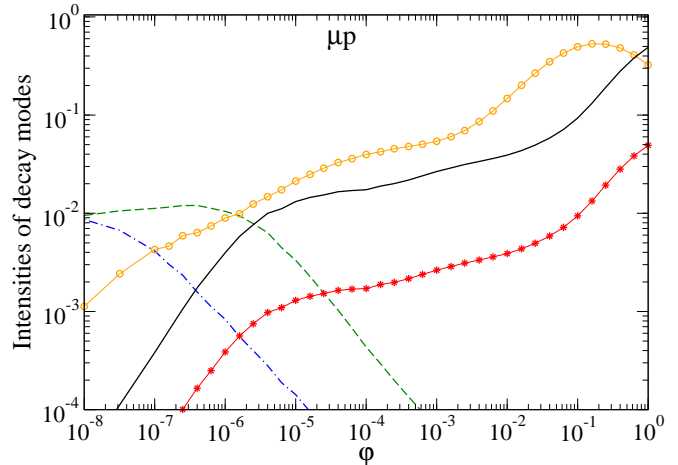


FIG. 7: Intensities (per one formed  $\mu^-p$  atom) for all disintegration modes of  $(\mu^-p)_{2s}$  vs the relative target density: collision-induced radiative quenching (solid line), Stark  $2s \rightarrow 2p$  transition (line with open circles), Coulomb de-excitation (line with asterisks), and  $\mu$ -decay (dashed and dashed-dotted lines for fractions below and above the  $2s - 2p$  threshold, respectively).

The figures and tables show the intensities of the following destruction modes:

- $I_{\text{Rqu}}$  - collision-induced radiative quenching,
- $I_{\text{Str}}$  - Stark transition  $2s \rightarrow 2p$  followed by the fast radiative  $2p \rightarrow 1s$  transition,
- $I_{\text{CD}}$  - Coulomb deexcitation  $2s \rightarrow 1s$ ,
- $I_\mu^a$  -  $\mu^-$ -decay at kinetic energies above the  $2s - 2p$  threshold,
- $I_\mu^b$  -  $\mu^-$ -decay at kinetic energies below the  $2s - 2p$  threshold.

At the lowest densities, the muon decay is the main process resulting in the disintegration of the  $2s$  state of both muonic hydrogen and deuterium atoms at kinetic energies above and below the  $2s - 2p$  threshold (see also Table II).

At kinetic energy above the  $2s - 2p$  threshold, the intensity of the  $\mu$ -decay decreases rather rapidly with the density increasing. On the contrary, the intensity of  $\mu$ -decay at kinetic energies below the  $2s - 2p$  threshold at first even increases with increasing density (especially in the case of  $(\mu^-d)_{2s}$ ) and then decreases rapidly with further increase in density at  $\varphi > 10^{-5}$ .

The intensities of Stark  $2s \rightarrow 2p$  transitions in muonic hydrogen and deuterium atoms are in accordance with

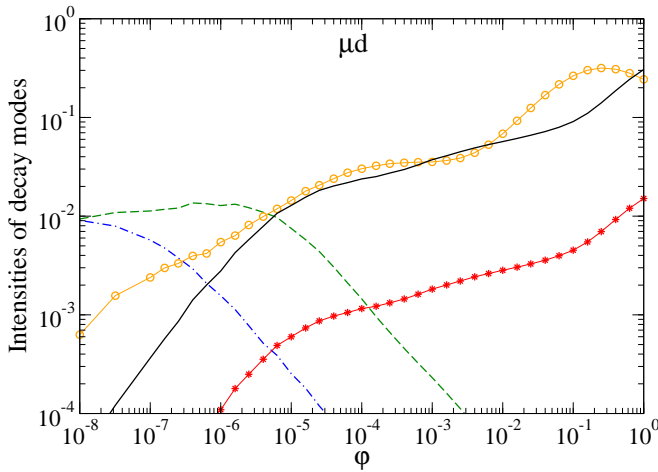


FIG. 8: The same as in Fig. 7 for  $(\mu^-d)_{2s} + D$  collisions.

TABLE II: The density dependence of intensities (per one formed muonic atom, in percent) of the  $\mu$ -decay calculated for  $(\mu^-p)_{2s}$  and  $(\mu^-d)_{2s}$  with kinetic energies both above and below the  $2s - 2p$  threshold ( $I_w^a$  and  $I_w^b$ , respectively).

$\varphi$ (lhd)	$(\mu^-p)_{2s}$		$(\mu^-d)_{2s}$	
	$I_w^a$	$I_w^b$	$I_w^a$	$I_w^b$
$10^{-8}$	0.86	0.95	0.91	0.95
$10^{-7}$	0.41	1.12	0.57	1.02
$10^{-6}$	0.08	1.05	0.16	1.43
$10^{-5}$	0.02	0.33	0.03	0.79
$10^{-4}$	0.00	0.04	0.00	0.14
$10^{-3}$	0.00	0.01	0.00	0.02

the primary populations of these atoms at kinetic energies above the  $2s - 2p$  threshold but turn out to be less than the values of the corresponding primary populations. The intensity of the Coulomb deexcitation for  $(\mu^-p)_{2s}$  are about 1.5 - 2 times higher than in the case of  $(\mu^-d)_{2s}$ , while the values of the radiation quenching intensity for these two isotopes are very close at the target density less than  $10^{-5}$  and with increasing density targets up to  $10^{-2}$  this ratio changes in favor of the muonic deuterium atom by about 1.5 times.

TABLE III: The density dependence of intensities  $I_{CD}$ ,  $I_{rqu}$ , and  $I_{Str}$  (in percent) calculated for  $(\mu^-p)_{2s}$  and  $(\mu^-d)_{2s}$ .

$\varphi$ (lhd)	$(\mu^-p)_{2s}$			$(\mu^-d)_{2s}$		
	$I_{CD}$	$I_{rqu}$	$I_{Str}$	$I_{CD}$	$I_{rqu}$	$I_{Str}$
$10^{-8}$	0.00	0.00	0.11	0.00	0.004	0.07
$10^{-7}$	0.004	0.04	0.43	0.00	0.04	0.27
$10^{-6}$	0.04	0.40	0.90	0.01	0.31	0.58
$10^{-5}$	0.13	1.32	2.13	0.06	1.36	1.48
$10^{-4}$	0.17	1.74	3.97	0.11	2.25	3.01
$10^{-3}$	0.26	2.66	5.41	0.18	3.70	3.55
$10^{-2}$	0.39	3.91	14.76	0.28	5.69	6.85
$10^{-1}$	0.94	9.33	49.52	0.45	9.09	26.45
$10^0$	4.93	48.98	32.38	1.51	30.59	24.33

The fastest collisional process – the elastic  $2s - 2s$  scattering – leads to a deceleration of muonic atoms in the  $2s$  state. As a result, some part of the muonic  $2s$ -state atoms initially formed with kinetic energies above the  $2s - 2p$  threshold turns out to be below the threshold. Thus, the population of the fraction with kinetic energy above the  $2s - 2p$  threshold decreases, and the population of the fraction with kinetic energy below the  $2s - 2p$  threshold increases accordingly compared to their values at the instant of formation. Thus, the total population of the fraction with kinetic energy below the  $2s - 2p$  threshold is always greater than its initial population  $\varepsilon_{2s}^b$ . This influence of elastic scattering on redistribution of fractions with kinetic energies above and below the  $3s - 2p$  threshold (in favor of increasing the sub-threshold fraction) increases with increasing target density.

In Table IV we present the initial population  $\varepsilon_{2s}^b$  and the total number of the disintegrated  $(\mu^-p)_{2s}$  atoms with the energy below the  $2s - 2p$  threshold  $I_{2s}^b$  (per one formed  $\mu^-p$  atom):

$$I_{2s}^b = I_{\mu}^b + I_{CD} + I_{rqu} \quad (11)$$

in comparison with the experimental data [6, 19].

TABLE IV: The initial population  $\varepsilon_{2s}^b$  and the total number of the disintegrated  $(\mu^-p)_{2s}$  atoms with the energy below the  $2s - 2p$  threshold  $I_{2s}^b$  (per one formed  $\mu p$  atom).

$\varphi$ (lhd)	$\varepsilon_{2s}^b$ (%)		$I_{2s}^b$ (%)		Ref.
	Theory	Theory	Theory	Exp.	
$7.35 \cdot 10^{-8}$	0.90	1.12	$0.85^{+0.14}_{-0.14}$		[6]
$2.94 \cdot 10^{-7}$	0.95	1.27	$0.92^{+0.08}_{-0.08}$		[6]
$1.18 \cdot 10^{-6}$	1.05	1.51	$1.10^{+0.08}_{-0.08}$		[6]
$4.71 \cdot 10^{-6}$	1.13	1.72	$1.25^{+0.98}_{-0.48}$		[19]
$1.88 \cdot 10^{-5}$	1.15	1.84	$1.07^{+0.57}_{-0.30}$		[19]
$7.53 \cdot 10^{-5}$	1.28	1.93	$1.63^{+1.08}_{-0.35}$		[19]

On the whole, there is a satisfactory agreement between the theoretical results and experimental data. An exception is the experimental value obtained at a target density of  $1.88 \cdot 10^{-6}$  [19], which is much less the corresponding theoretical value. It should be noted that this experimental value falls out of the general trend of population growth with increasing target density and, moreover, there are no arguments to explain it.

#### D. Absolute x-ray yield of $K\alpha$ line

The absolute x-ray yield of the  $K\alpha$  line is determined as the intensity of this line per muonic atom formed. The total intensity,  $I_{K\alpha}$ , of the  $K\alpha$  line can be represented as a sum of three different contributions corresponding to the preceding history of the atoms involved in its formation:

$$I_{K\alpha} = I_{2p \rightarrow 1s} + I_{Str} + I_{rqu}. \quad (12)$$

Here  $I_{2p \rightarrow 1s}$  denotes the intensity of the direct  $2p \rightarrow 1s$  radiative transition occurring after the transition of a

muonic atom to the  $2p$  state from states with the principal quantum number  $n \geq 3$ . Remind, that  $I_{\text{Str}}$  and  $I_{\text{rqu}}$  are the intensities of the  $2s \rightarrow 2p$  Stark transition (at kinetic energies above the  $2s - 2p$  threshold) followed by the  $2p \rightarrow 1s$  radiative transition and the collision-induced radiative quenching of the  $2s$  state (at kinetic energies below the  $2s - 2p$  threshold), respectively.

Figures 9 and 10 show the density dependence of the different modes forming the total absolute yield of the  $K\alpha$  line as well as their sum calculated at a target temperature  $T = 300$  K for  $\mu^-p$  and  $\mu^-d$  atoms, respectively.

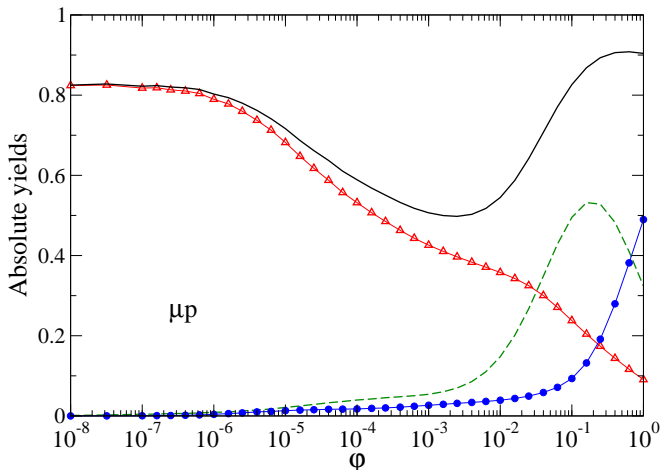


FIG. 9: The density dependence of the different contributions to the absolute  $K\alpha$ -line yield calculated for muonic hydrogen at the target temperature  $T = 300$  K.:  $I_{2p \rightarrow 1s}$  (solid line with triangles),  $I_{\text{Str}}$  (dashed line),  $I_{\text{rqu}}$  (solid line with filled circles), and their sum (solid line).

As can be seen from Figures 9 and 10, the contribution of the direct radiation  $2p - 1s$  transition  $I_{2p \rightarrow 1s}$  to the absolute yield of the  $K\alpha$ -line decreases with increasing target density  $\varphi > 10^{-6}$ . In the case of a muonic hydrogen atom, this decrease becomes rather rapid at  $\varphi > 10^{-3}$  and the contribution reaches a value of 0.1 at the density of liquid hydrogen. In the case of a muonic deuterium atom, we observe a similar dependence on the density at  $\varphi < 10^{-3}$ , however a further increase in the target density does not lead to a sharp decrease of the contribution  $I_{2p \rightarrow 1s}$  (at the density of liquid hydrogen, this contribution is about 0.4). This difference in the dependence of  $I_{2p \rightarrow 1s}$  on the density in muonic hydrogen and muonic deuterium is explained by isotope effect in the rates of collisional processes of these atoms (see [5]) in the upper part of the cascade of deexcitation ( $n \geq 3$ ). In particular, this is reflected in the primary populations of the  $2s$  state at kinetic energies above the  $2s - 2p$  threshold (see Table I).

### E. Probabilities of different disintegration modes and lifetime of $(\mu^-p)_{2s}$ and $(\mu^-d)_{2s}$

The probability that the muonic atom formed in the  $2s$  state disintegrates due to one of decay modes,  $P_i(\varphi)$ ,

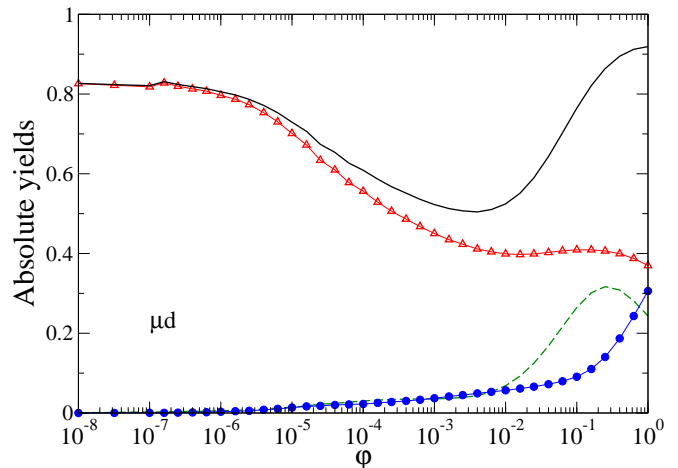


FIG. 10: The same as in Fig. 9 for  $\mu^-d$  atom.

is given by

$$P_i(\varphi) = \frac{1}{p_0} \left\{ 1 - \exp \left[ - \int_0^\infty \frac{\lambda_i(E; \varphi)}{\lambda_{\text{tot}}(E; \varphi)} F_i(E; \varphi) dE \right] \right\}. \quad (13)$$

Here, the  $\lambda_i(E; \varphi)$  is the rate of the process  $i$  where index  $i$  denotes the following disintegration channels:  $i = \mu$  ( $\mu$ -decay),  $i = \text{CD}$  (Coulomb deexcitation  $2s \rightarrow 1s$ ),  $i = \text{rqu}$  (collision-induced radiative quenching), and  $i = \text{Str}$  (Stark transition  $2s \rightarrow 2p$  resulting in the radiative transition  $2p \rightarrow 1s$ ).  $\lambda_{\text{tot}}(E; \varphi)$  is a summary rate of all processes, which lead to the disintegration of the  $2s$  state:

$$\lambda_{\text{tot}}(E; \varphi) = \lambda_\mu + \lambda_{\text{CD}} + \lambda_{\text{rqu}} + \lambda_{\text{Str}}. \quad (14)$$

The factor  $p_0 = 1 - e^{-1}$  provides the correct behavior of the probability  $P_\mu$  in the limit  $\varphi \rightarrow 0$ . The kinetic energy distribution  $F_i(E; \varphi)$  is defined at the instant of the disintegration of the  $2s$  state through the  $i$ -th decay mode and normalized by the condition:

$$\int_0^\infty F_i(E; \varphi) dE = 1. \quad (15)$$

The probability of the different disintegration modes for  $(\mu^-p)_{2s}$  and  $(\mu^-d)_{2s}$  atoms as functions on target density is shown in Figures 11 and 12, correspondingly. As can be seen from the figures, probabilities of  $\mu$ -decay have a similar density dependence for muonic hydrogen and deuterium atoms. This is explained by the fact that the  $\mu$ -decay rate does not depend on either the energy or the target density, and the kinetic energy distributions of muonic hydrogen and deuterium are very close in the density region where the probability of muon decay is not negligible (see Fig. 5).

On the contrary, for the probabilities of the destruction of the  $2s$  state in collisional processes, we observe significant differences between muonic hydrogen and deuterium in both the values of these probabilities and their dependence on the target density. These differences are especially pronounced in the ratio of the probabilities of Stark transitions and collision-induced radiation quenching. The observed differences are explained by two factors: significant differences in the ratio of velocities, as



well as in the distributions over the kinetic energies of muonic hydrogen and deuterium atoms.

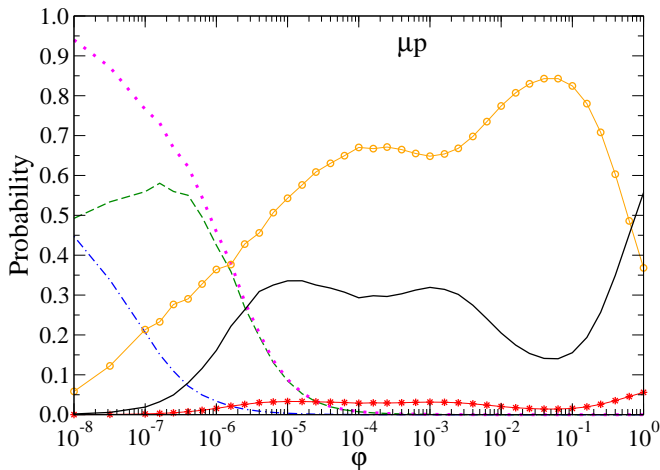


FIG. 11: The density dependence of decay probabilities of  $(\mu^-p)_{2s}$  for various disintegration modes: collision-induced radiative quenching (solid line), Stark  $2s \rightarrow 2p$  transition (line with open circles), Coulomb de-excitation (line with asterisks), and  $\mu$ -decay (dashed and dashed-dotted, and dotted lines for fractions below and above the  $2s - 2p$  threshold and their sum, respectively).

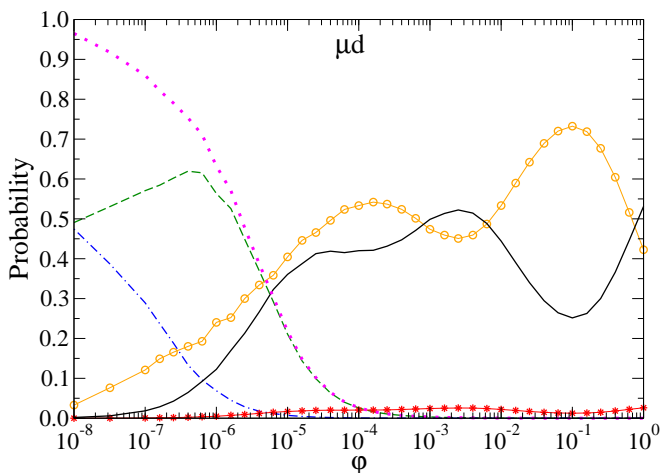


FIG. 12: The same as in Fig. 11 for  $(\mu^-d)_{2s}$  atom.

The mean time interval between the formation of the muonic atom in the  $2s$  state and its decay we define as the lifetime of the  $2s$  state. In this work, to determine the lifetime of the  $2s$  state, we use the  $\mu$ -decay probability

$$P_\mu(\varphi) = \frac{1}{p_0} [1 - \exp(-\lambda_\mu \tau_{2s}(\varphi))], \quad (16)$$

where a lifetime  $\tau_{2s}(\varphi)$  of the  $2s$  state is defined by

$$\tau_{2s}(\varphi) = \int_0^\infty \frac{F_\mu(E; \varphi)}{\lambda_{\text{tot}}(E; \varphi)} dE \quad (17)$$

From Eqs. (16) and (17) we obtain

$$\tau_{2s}(\varphi) = -\tau_\mu \ln [1 - p_0 \cdot P_\mu(\varphi)]. \quad (18)$$

Formulas similar to Eqs. (16)-(18) allow to define and to calculate the lifetime  $\tau_{2s}^a$  for the fraction of atoms in the  $2s$  state with the kinetic energy above the  $2s - 2p$  threshold and also the lifetime  $\tau_{2s}^b$  for the fraction of atoms in the  $2s$  state with the kinetic energy below the  $2s - 2p$  threshold.

$$P_\mu^\alpha(\varphi) = \frac{1}{p_0} [1 - \exp(-\lambda_\mu \tau_{2s}^\alpha(\varphi))], \quad (19)$$

where

$$\tau_{2s}^\alpha(\varphi) = \int_0^\infty \frac{F_\mu^\alpha(E; \varphi)}{\lambda^\alpha(E; \varphi)} dE. \quad (20)$$

is the lifetime of the fraction of the  $2s$  state with the kinetic energy above ( $\alpha = a$ ) or below ( $\alpha = b$ ) the  $2s - 2p$  threshold, respectively. The corresponding total rates of these fractions are given by:

$$\lambda^a(E; \varphi) = \lambda_\mu + \lambda_{\text{CD}}(E; \varphi) + \lambda_{\text{str}}(E; \varphi) \quad (21)$$

and

$$\lambda^b(E; \varphi) = \lambda_\mu + \lambda_{\text{CD}}(E; \varphi) + \lambda_{\text{rqu}}(E; \varphi). \quad (22)$$

Infinite limits of integration in Eq. (20) are of a formal nature, since the probability densities  $F_\mu^a(E; \varphi)$  and  $F_\mu^b(E; \varphi)$  are different from zero only in the intervals  $E \geq E_{\text{thr}}$  and  $E \leq E_{\text{thr}}$ , respectively. From Eqs. (19) and (20) we obtain

$$\tau_{2s}^\alpha(\varphi) = -\tau_\mu \ln [1 - p_0 \cdot P_\mu^\alpha(\varphi)]. \quad (23)$$

In the present study three variants of the  $(\mu^-p)_{2s}$  and  $(\mu^-d)_{2s}$  lifetime were calculated: the lifetime,  $\tau_{2s}^a$ , of the fraction with the kinetic energy above the  $2s - 2p$  threshold, the lifetime,  $\tau_{2s}^b$ , of the fraction with the kinetic energy below the  $2s - 2p$  threshold, and the lifetime,  $\tau_{2s}$ , of the  $2s$  state independently whether the kinetic energy of muonic atom is above or below the  $2s - 2p$  threshold.

Results of calculations are presented in Figs. 13 and 14 for the  $(\mu^-p)_{2s}$  and  $(\mu^-d)_{2s}$  atoms, respectively. As it is seen from the figures, the lifetime of the  $2s$  state for both muonic hydrogen and muonic deuterium has a similar dependence on density for both fractions. At the lowest densities, the lifetimes are determined by the muon decay rate. With increasing density, the role of collisional processes increases, which leads to a decrease in the lifetime of both fractions. The lifetime for the fraction with kinetic energy below the  $2s - 2p$  threshold,  $\tau_{2s}^b$ , decreases much more slowly with increasing target density than for the fraction with kinetic energy above the  $2s - 2p$  threshold. At a densities  $\varphi > 10^{-5}$ , the lifetime of a  $2s$  state behaves as  $\varphi^{-1}$ , and the ratio  $\tau_{2s}^b/\tau_{2s}^a$  is equal to about 15.

In the case of muonic hydrogen, the theoretical values of the lifetime of the fractions with kinetic energy both above and below the  $2s - 2p$  threshold are in excellent agreement with the available experimental data. In the case of muonic deuterium, the agreement between the theoretical and available at one density experimental values of the lifetimes of the  $2s$  state can be considered as good for  $\tau_{2s}^b$  and satisfactory for  $\tau_{2s}^a$ .

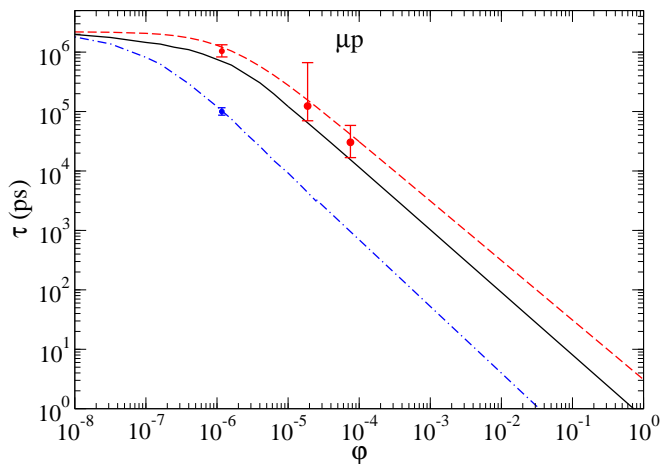


FIG. 13: The density dependence of the  $(\mu^-p)_{2s}$  lifetime calculated for various fractions: below the  $2s-2p$  threshold - dashed line, above the  $2s-2p$  threshold - dashed-dotted line. The lifetime,  $\tau_{2s}$ , of the  $2s$  state independently whether the kinetic energy of muonic atom is above or below the  $2s-2p$  threshold is shown by the solid line. The experimental values from [19]

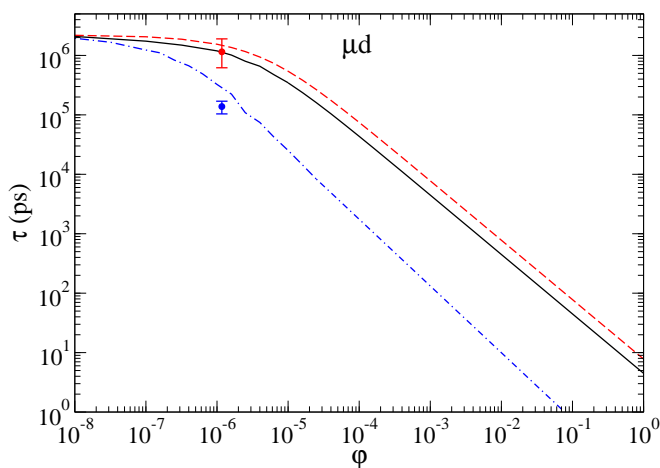


FIG. 14: The same as in Fig. 13 for  $(\mu^-d)_{2s}$ . The experimental values from [22]

#### IV. CONCLUSION

The fully quantum-mechanical study of the collisional processes — elastic scattering, collision-induced radiative quenching, and Coulomb deexcitation — has been performed in the framework of the close-coupling approach for  $(\mu^-p)_{2s}+H$  and  $(\mu^-d)_{2s}+D$  collisions at kinetic energies below the  $2s-2p$  threshold. The cross sections have been calculated with the basis set including all open and closed channels associated with the exotic atom states with the principal quantum number up to  $n_{max} = 30$  and then have been used as input data in the kinetics of the atomic cascade.

An important result of this work is the elucidation of the role of the collision-induced radiative quenching in the destruction of a muonic atom in  $2s$ -state. As far as the authors know, this problem has not been previously investigated. Our calculations showed that this process makes a significant contribution to the total disintegration of the  $2s$ -state of muonic atoms at energies below the  $2s-2p$  threshold.

The kinetics of the atomic cascade has been investigated for both muonic hydrogen and muonic deuterium atoms within the updated version of the cascade model, which has a number of essential improvements over the previous cascade calculations. The cascade calculations have been performed for target densities covering eight orders of magnitude from  $10^{-8}$  up to 1 (in the units of the liquid hydrogen density).

As a result of *ab initio* cascade calculations, a number of characteristics of the  $2s$  state of muonic hydrogen and deuterium atoms were obtained: primary populations and kinetic energy distributions, absolute values of intensities different modes of disintegration, the probability of decay of the  $2s$  state through different channels and lifetimes of the  $2s$  state at kinetic energy both above and below the  $2s-2p$  threshold. The obtained theoretical results are compared with the available experimental data. The results of the work can be used for the planning experiments and analysis of experimental data.

- 
- [1] G. Ya. Korenman and V. P. Popov, Muon Catalyzed Fusion **4**, 145 (1989).  
 [2] G. Ya. Korenman, V. P. Popov, and G. A. Fesenko, Muon Catalyzed Fusion **7**, 179 (1992).  
 [3] J. S. Cohen, Rep. Prog. Phys. **67**, 1769 (2004).  
 [4] V. P. Popov and V. N. Pomerantsev, Phys. Rev. A **83**, 032516 (2011).  
 [5] V. P. Popov and V. N. Pomerantsev, Phys. Rev. A **95**, 022506 (2017).  
 [6] R. Pohl, Ph.D. thesis 14096, ETH Zurich, 2001.  
 [7] R. Pohl, H. Daniel, F.J. Hartmann et al., PRL **97**, 193402 (2006).  
 [8] J. Wallenius, S. Jonsell, Y. Kino and P. Froelich, Hyperfine Interact. **138**, 285 (2001).  
 [9] R. Pohl et al., Hyperfine Interact. **138**, 35 (2001).  
 [10] P. O. Egan et al., Phys. Rev. A **23**, 1152 (1981).  
 [11] H. Anderhub et al., Phys. Lett. B **143**, 65 (1984).  
 [12] N. Bregant et al., Phys. Lett. A **241**, 344 (1998).  
 [13] F. Kottman et al., Hyperfine Interact. **119**, 3 (1999); **138**, 55 (2001).  
 [14] G. Kodosky and M. Leon, Nuovo Cimento **B1**, 41 (1971).  
 [15] R. O. Mueller, V. W. Hughes, H. Rosenthal, and C. S. Wu, Phys. Rev. A **11**, 1175 (1975).  
 [16] G. Carboni and G. Fiorentini, Nuovo Cimento **B39**, 281 (1977).  
 [17] James S. Cohen and J. N. Bardsley, Phys. Rev. A **23**, 46 (1981).  
 [18] T. S. Jensen and V. E. Markushin, Eur. Phys. J. **D 21**, 271 (2002).  
 [19] Randolph Pohl et al., Phys. Rev. Lett. **97**, 193402 (2006).  
 [20] L. Ludhova et al., Phys. Rev. A **75**, 040501(R) (2007).  
 [21] R. Pohl et al., Nature (London) **466**, 213 (2010).  
 [22] Marc Diepold et al., Phys. Rev. A **88**, 042520 (2013).  
 [23] Pomerantsev Vladimir N., Popov Vladimir P., Hyperfine Interact. **209**, 75 (2012).  
 [24] G. Ya. Korenman, V. N. Pomerantsev, and V. P. Popov, JETP Lett. **81**, 543 (2005).  
 [25] V. N. Pomerantsev and V. P. Popov, JETP Lett. **83**, 331

- (2006).
- [26] V. N. Pomerantsev and V. P. Popov, Phys. Rev. A **73**, 040501(R) (2006).
- [27] Pomerantsev Vladimir N., Popov Vladimir P., Hyperfine Interact. **209**, 69 (2012).
- [28] V. P. Popov and V. N. Pomerantsev , Phys. Rev. A **86**, 052520 (2012).